Chapter 9
Real-Time Implementation of an ISM Fault Tolerant Control Scheme on the SIMONA Flight Simulator

This chapter describes the results of implementing the LPV integral sliding mode FTC controller from Chap. 8 on the 6-DOF SIMONA motion flight simulator at Delft University of Technology. This demonstrates proof of concept in a realistic operational environment, and shows the applicability of the integral sliding mode FTC scheme. The LPV FTC scheme has been evaluated with a pilot-in-the-loop to give insight into real-time performance issues, and to assess the effect on the handling of the aircraft in nominal and in fault/failure scenarios.

9.1 SIMONA Research Simulator (SRS)

The SIMONA (SImulation, MOtion and NAvigation) research simulator (SRS) (Fig. 9.1) is a realistic 6 degree-of-freedom pilot-in-the-loop flight simulator located at Delft University of Technology. The SRS has a typical commercial aircraft cockpit with two side-by-side pilot seats, and typical pilot controls (a hydraulically activated control column, electrically actuated side stick, a rudder pedal (from an actual B777 aircraft), control wheel, thrust lever, flap and landing gear lever). At the centre of the cockpit is a mode control panel (MCP) from a B737 (Fig. 9.2), to allow auto-pilot commands and configuration selection, as well as an electronic flight control display (which can be configured to represent any aircraft display) to provide pilots with typical flight information such as control surface deflections and the aircraft trajectory. The SRS has an outside virtual world projection which can be set to any location. The SRS 180 $\times$ 40 deg outside visual field of view is supplied by three LCD projectors and provides the pilot with an immense sense of motion and the attitude of the aircraft. The motion of the SRS is provided by 6 large hydraulic hexapods and the SRS motion cueing algorithm, allowing any aircraft dynamics and manoeuvres to be implemented. The SRS is operated by a network of modular computers, each with a different function and task (visual cuing, motion control, running the aircraft model, data logging, control load feel, and the flight control computer).

M.T. Hamayun et al., *Fault Tolerant Control Schemes Using Integral Sliding Modes*, Studies in Systems, Decision and Control 61,
DOI 10.1007/978-3-319-32238-4_9

Fig. 9.1 SIMONA research simulator (picture courtesy of Delft University of Technology)

Communication and synchronisation between the different computers in the network are provided by high speed fibre optic cables. The custom-built motion and visualisation system, and its modular structure allow the SRS to be configured to represent any aircraft and has the capability of implementing any existing or 'experimental' flight control scheme. In this chapter, the SRS has been configured to represent the RECOVER B747-100/200 aircraft[1] with an outside virtual world representation of the area around Amsterdam-Schiphol airport. This SRS configuration is programmed using DUECA (Delft University Environment for Communication and Activation). The DUECA software architecture also handles the real-time scheduling, and ensures that each of the computers are synchronised.

[1] For details of the RECOVER benchmark model see the Appendix A.1.

Fig. 9.2 Mode Control Panel (MCP)

9.2 Design and SRS Implementation

This chapter considers the design of the adaptive ISM controller given in Chap. 8 and its implementation on the SRS. It is assumed that a measurement of the actual actuator deflections are available. Furthermore, the monitoring channels are separate from the control channels, and so faults in the actuators do not affect the fidelity of the control surface monitoring signals. In these experiments the diagonal elements $\hat{w}_i(t)$ of $\widehat{W}(t)$ in (8.53) have been estimated based on a least squares approach using information provided by the actual actuator deflections and the command signals from the controller.

9.2.1 SRS Implementation

The LPV design discussed in Sect. 8.3 is only associated with the longitudinal axis, although a lateral axis controller[2] must also be incorporated for the purpose of testing and evaluation. However the description of the SRS implementation will only focus on the longitudinal controller. In this chapter, the controller has been initially developed and tuned using MATLAB V2006b (the original version supported by the RECOVER model) using an ODE4 fixed time step solver with a step size of 0.01 s. For the implementation, the SIMULINK model of the designed ISM controller (which has the GARTEUR FM-AG16 standardised inputs–outputs in order to fit with the SRS implementation) has been converted to C code using the MATLAB Real-Time Workshop(R) utility. The C coded controller is then implemented on a PC with an Intel(R) Xeon(R) 3.07 GHz processor which has been used as the flight control computer. However the computational load measured as the time needed for a single integration step on the flight computer was found to be 0.15 msec. Figure 9.3 shows the overall controller configuration and the interface to the SRS, where it is clear that the inner-loop longitudinal controller provides flight path and speed tracking, which the pilot can command directly using the MCP dials at the centre of the cockpit. The outer-loop longitudinal controller provides altitude control using a simple PID scheme to provide a flight path angle command to the inner-loop ISM controller. In the results which follow $K_{p_{FPA}} = 0.1$, $K_{i_{FPA}} = 0.07$ and $K_{d_{FPA}} = 0.1$.

[2] See [1] for details of the lateral controller.

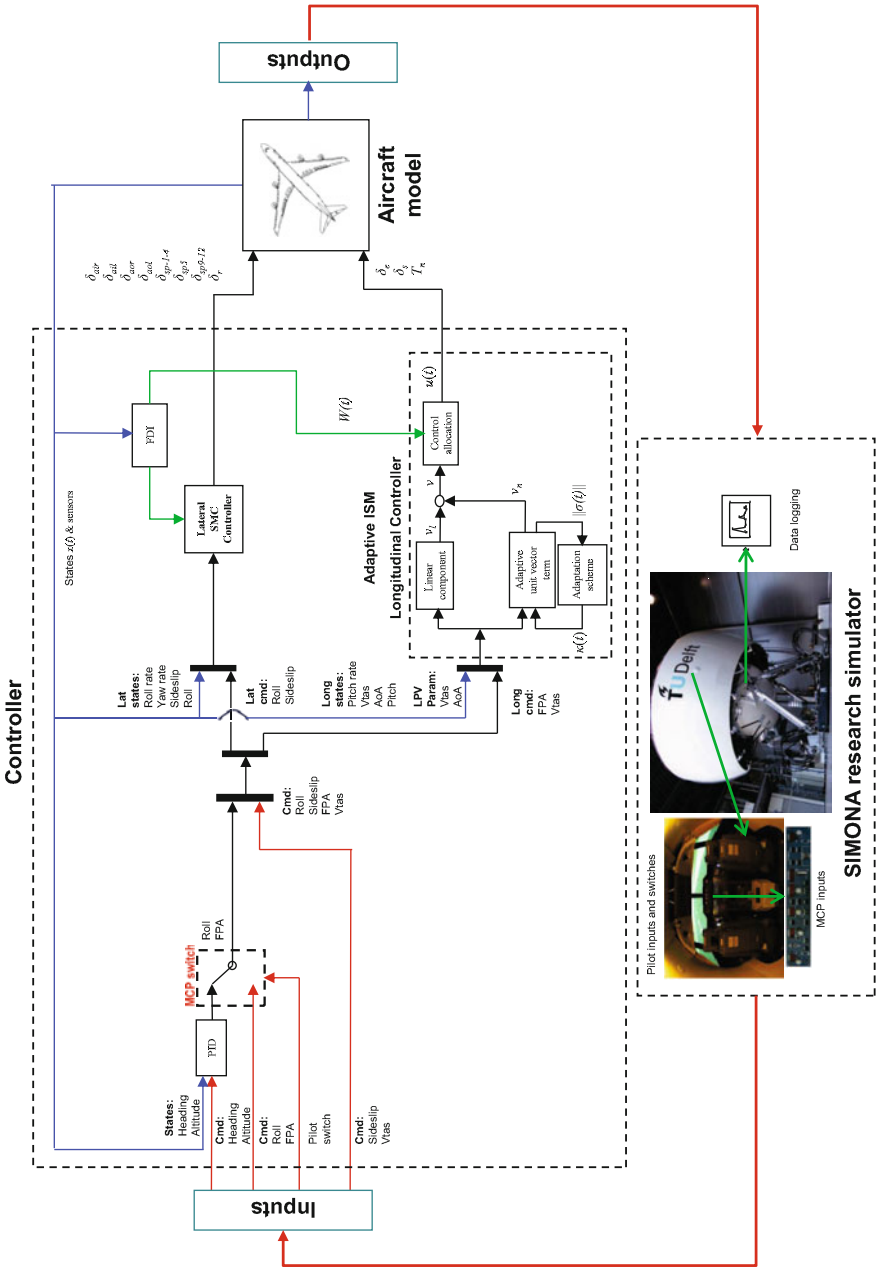

Fig. 9.3 Controller interconnection

9.3 SRS Piloted Evaluation Results

The results in this section represent evaluation tests by an experienced commercial pilot. Figure 9.4 shows the overall manoeuvres for three different tests: fault-free, elevator jam and stabiliser runaway. The following describes the sequence of manoeuvres conducted during the pilot evaluation:

1. Straight and level flight at 250 kts (128.6 m/s), 2000 ft (609.6 m) heading North.
2. Insert failure (for failure cases).
3. Right turn 90 deg (East).
4. Left turn back to 0 deg (North).
5. Altitude change to 4000 ft (1219.2 m).
6. Altitude change back to 2000 ft (609.6 m).
7. Acceleration to 300 kts (154.3 m/s) (indicated air speed).
8. Deceleration to 250 kts (128.6 m/s) (indicated air speed).
9. Deceleration to 228 kts (117.3 m/s) (indicated air speed).

Note that each manoeuvre was allowed to reach steady state before the next sequence was tested.

The controller has been tested at the trim condition

$$(5.53\ \text{deg},\ 0.0017\ \text{deg/s},\ 133.8\,\text{m/s},\ 5.53\ \text{deg},\ 600\,\text{m})$$

with an input trim (2 deg, -1.59 deg, 45568 N) with an initial mass of 317,000 kg and with the flaps fully retracted. This represents one of the trim conditions used

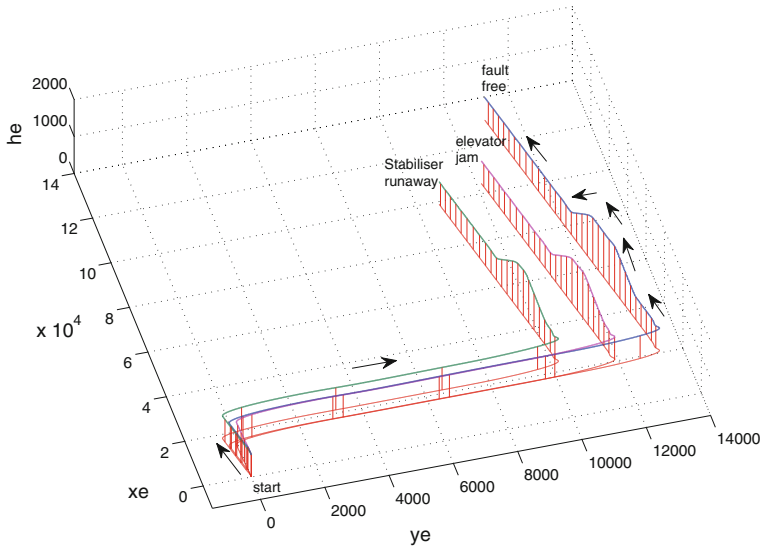

Fig. 9.4 Pilot evaluation: Trajectory

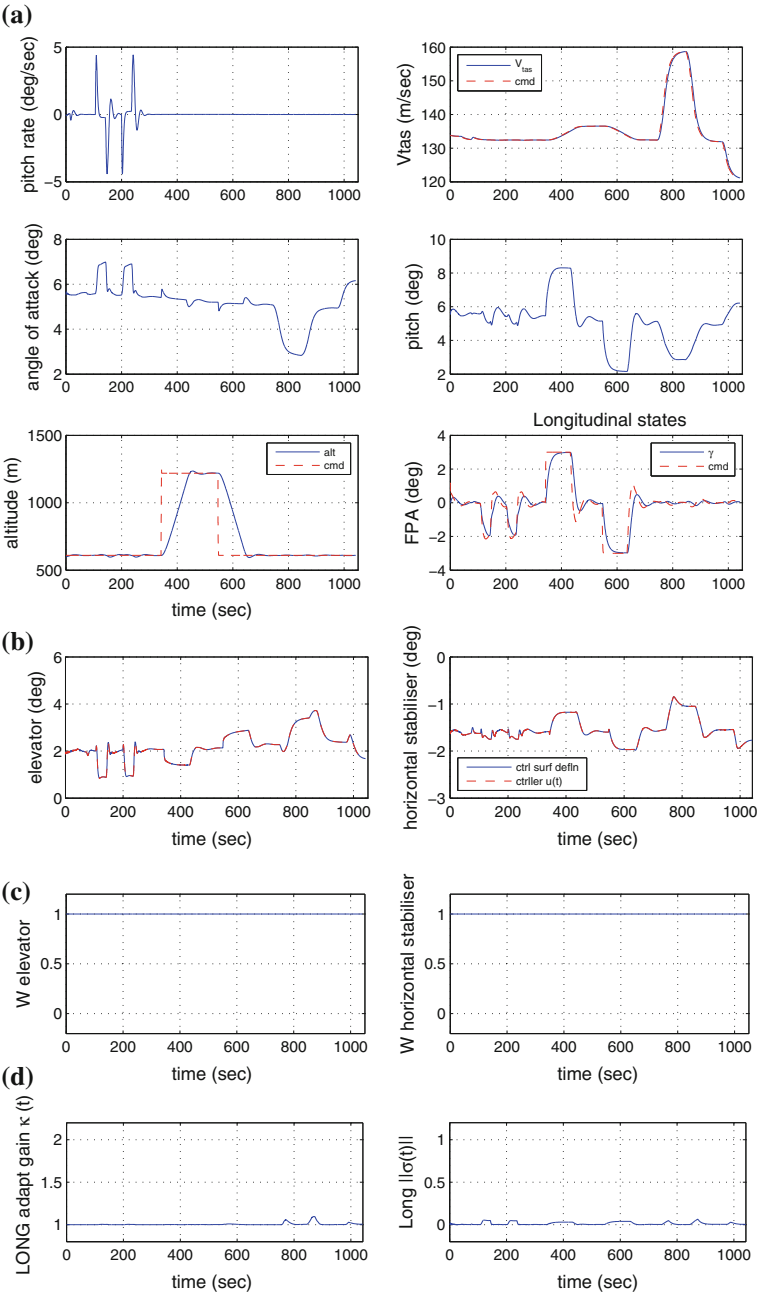

Fig. 9.5 Pilot evaluation—fault-free longitudinal performance. **a** Longitudinal states, **b** Longitudinal control surfaces, **c** control surface effectiveness estimation, **d** switching function and adaptive gain

for the GARTEUR FM-AG16 benchmark problem and it is different to the trim conditions of the LPV model in Appendix A.1.1. Using different flight conditions for the evaluation highlights the capability of the designed controller to operate in regions away from the design point.

Remark 9.1 Note that the aircraft trajectories for the three different tests in Fig. 9.4 are not identical. This is due to the fact that the manoeuvres were 'manually' flown by the pilot using the mode control panel. Although the magnitudes of the heading, altitude and speed commands are the same, the times at which each manoeuvre is executed are different.

9.3.1 Fault-Free

Figure 9.5 shows longitudinal fault-free performance. The longitudinal states and the tracking performance is shown in Fig. 9.5a. Figure 9.5b shows the control surface deflections during nominal fault-free conditions. Figure 9.5c shows that no fault/failure is present in the elevator or stabiliser (the actuator effectiveness is $W(t) = 1$ for both surfaces). Finally Fig. 9.5d shows the nominal variation in the switching function and the adaptive gain due to changes in the operating conditions.

9.3.2 Elevator Jam

Figure 9.6 shows the pilot evaluation for the case of an elevator jam. Figure 9.6c shows the elevator failure occurred at approximately 63 s when the effectiveness level drops to zero. The effect of the elevator jam can be seen in Fig. 9.6b. After this point in time, the stabiliser becomes more active in order to compensate for the jammed elevator. Despite the presence of a failure, Fig. 9.6a shows similar state tracking performance as the fault-free case. Finally Fig. 9.6e shows the switching function is still close to zero indicating sliding is still maintained. Figure 9.6d shows a magnified portion of the estimate of the elevator effectiveness levels in the case of the elevator fault in Fig. 9.6c. Figure 9.6d shows that the estimation provided by the FDI scheme considered in this chapter[3] is not perfect, and includes detection delays (arising from the moving window of information and the filters employed to ensure a usable estimate of the actuator effectiveness levels).

[3] See page 265 of [2].

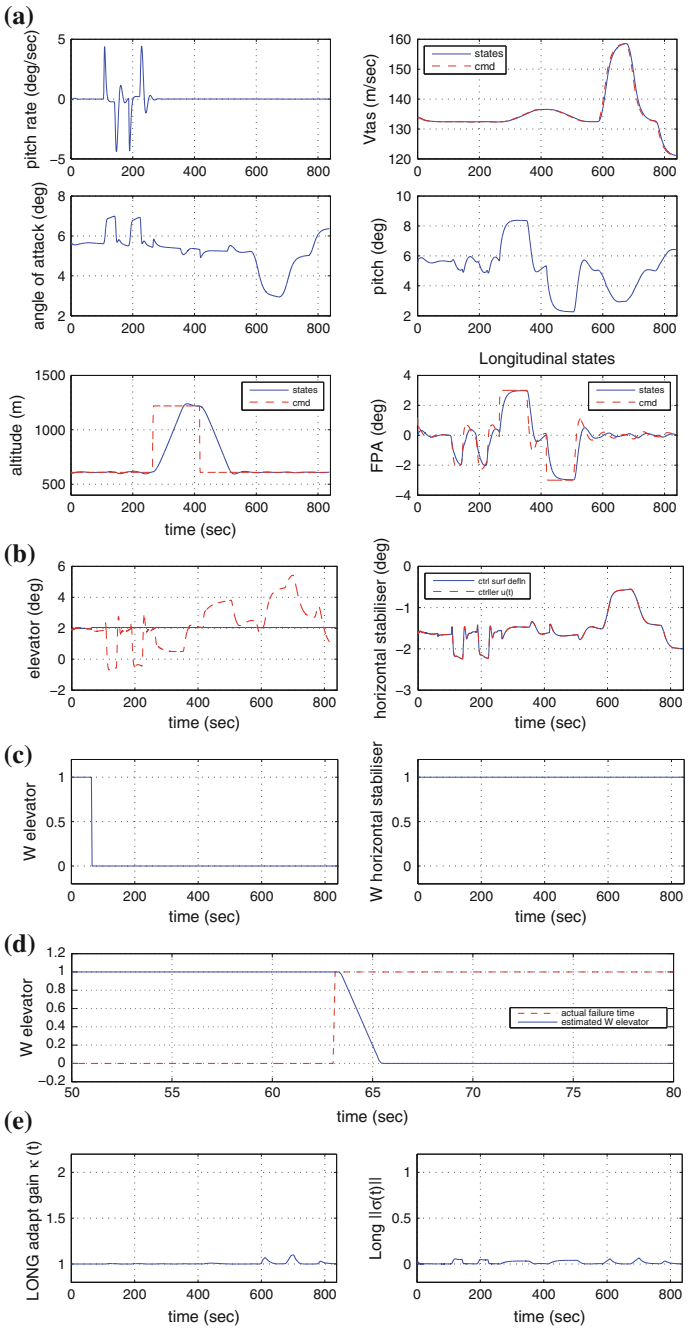

Fig. 9.6 Pilot evaluation—Elevator jam. **a** states, **b** control surfaces, **c** control surface effectiveness estimation, **d** zoomed in elevator estimated effectiveness level estimation

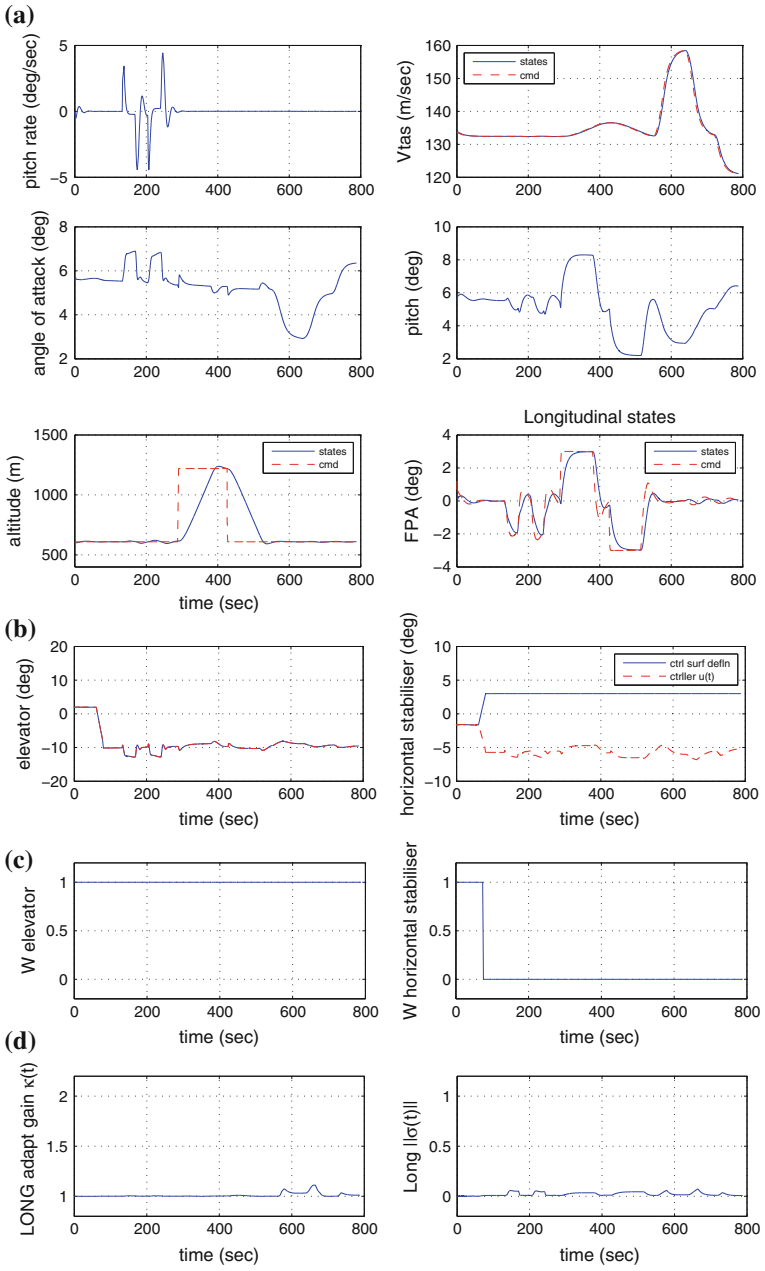

Fig. 9.7 Pilot evaluation: Stabiliser runaway. **a** states, **b** control surfaces, **c** control surface effectiveness estimation, **d** switching function and adaptive gain

9.3.3 Stabiliser Runaway

Figure 9.7 shows the evaluation results for the more challenging case of a stabiliser runaway at approximately 74 s (see Fig. 9.7c). The effect of the stabiliser runaway can be seen in Fig. 9.7b, where the stabiliser runs-away at its maximum rate to the maximum physical limits of 3 deg. Figure 9.7b also shows the deflection of the elevator to approximately −10 deg immediately after the stabiliser saturates in order to compensate for the stabiliser runaway. Despite the presence of this critical failure, Fig. 9.7a shows hardly any noticeable difference in terms of state tracking performance as compared to the fault-free case. Figure 9.7d shows that sliding is still being maintained, and the adaptive gain remains low.

9.3.4 Pilot Feedback

The following observations and discussions represent feedback from the pilot and the SRS researcher conducting the evaluation for all the three scenarios. Generally, the feedback from the pilot and the SRS researcher indicates that all three tests (nominal, the elevator jam and the stabiliser runaway) showed very similar performance and the pilot was unable to discern a meaningful difference, without looking at the surface deflections. The pilot reported that no transients were observed at the time of the failures. (In fact the SRS researcher had to double check that failures had actually occurred).

Some specific comments from the pilot and SRS researcher on the performance of the longitudinal controller are:

- Speed capturing was satisfactory, with some creep towards the set speed at the end.
- Altitude change capturing resulted in a rather careful 1400 feet (426.7 m) per minute rate for a 2000 ft (609.6 m) change. A rule of thumb is 2000 ft per minute (609.6 m per minute) for a 2000 ft change. A small overshoot of 60 ft (18.3 m) was observed on both climb and descent, which though not excessive, would not be acceptable in practice. The altitude set point was passed at around 600 ft (182.8 m) per minute. The subsequent undershoot of 20 ft (6.1 m) is also not desirable. A first-order response with no over or undershoot is desirable, rather than the current damped second order response.
- Speed tracking was acceptable during the manoeuvres (1 or 2 kts (0.51 or 1.03 m/s) deviations were observed, which is acceptable).
- Altitude tracking was generally good, apart from the small 40 ft (12.2 m) drop during heading capture.

9.4 Summary

This chapter has presented the results from real-time implementation and testing of the LPV based adaptive FTC scheme described in Chap. 8, on the SIMONA research simulator. The integral sliding mode approach ensures ideal sliding throughout the closed-loop system response, and maintains near to nominal performance in the face of actuator faults/failures. The scheme also takes into account imperfect estimation of the actuator effectiveness levels and considers an adaptive gain in the nonlinear component of the control law, to account for the imperfect estimation of the actuator effectiveness levels. The FTC scheme has been implemented and evaluated in a realistic operational environment with a pilot-in-the-loop. Evaluation results from the SIMONA research simulator show good tracking performance even in the event of faults/failures.

9.5 Notes and References

The SIMONA research simulator is a powerful tool and serves as a proof of concept test-bed in various research areas, for example: research into human-machine interaction [3], human motion perception [4–6], air traffic control [7], flight procedures [8, 9], aircraft handling qualities [10, 11], fly-by-wire control algorithms and flight deck displays [12, 13]. The SRS has been used to evaluate the real-time performance of different fault tolerant control algorithms in a pilot-in-the-loop configuration, considering the real EL AL flight 1862 accident scenario [14, 15]. A re-enactment of this incident was considered and implemented on the SIMONA research simulator in [16, 17]. In [16], a sliding mode FTC scheme using a fixed control allocation structure was tested whereas in [17], an adaptive nonlinear dynamic inversion approach was used for manual fly-by-wire control. Adaptive sliding mode FTC schemes were proposed in [18] where both fixed and online control allocation structures were compared by implementing them both in a piloted simulator environment. Recently in [19], propulsion-control tests were conducted on SIMONA, considering the failure of all control surfaces. The proposed fault tolerant sliding mode control allocation scheme in [19] was shown to be capable of dealing with the loss of all control surfaces and was able to achieve a safe emergency landing using only the engines.

References

1. Alwi, H., Edwards, C., Stroosma, O., Mulder, J.A.: Evaluation of a sliding mode fault-tolerant controller for the EL AL incident. AIAA j. Guid. Control Dyn. **33**(3), 677–694 (2010)
2. Alwi, H., Edwards, C., Tan, C.P.: Fault Detection and Fault Tolerant Control Using Sliding Modes. Advances in Industrial Control Series. Springer, London (2011)

3. Stroosma, O., Paassen, R.V., Mulder, M.: Using the SIMONA research simulator for human-machine interaction research. In: AIAA Modeling and Simulation Technologies Conference (2003)
4. Heerspink, H.M., Berkouwer, W.R., Stroosma, O., Paassen, R.V., Mulder, M., Mulder, J.: Evaluation of vestibular thresholds for motion detection in the SIMONA research simulator. In: AIAA Modeling and Simulation Technologies Conference (2005)
5. Valente Pais, A.R., Mulder, M., Paassen, R.V., Wentink, M., Groen, E.L.: Modeling human perceptual thresholds in self–motion perception. In: AIAA Modeling and Simulation Technologies Conference (2006)
6. Zaal, P.M.T., Nieuwenhuizen, F.M., Mulder, M., Paassen, R.V.: Perception of visual and motion cues during control of self–motion in optic flow environments. In: AIAA Modeling and Simulation Technologies Conference (2006)
7. Vormer, F.J., Mulder, M., Paassen, R.V., Mulder, J.: Optimization of flexible approach trajectories using a genetic algorithm. J. Aircr. **43**, 941–952 (2006)
8. De Gaay, W.F., Paassen, R.V., Mulder, M., In't Veld, A.C., Clarke, J.P.: Implementing time-based spacing for decelerating approaches. J. Aircr. **44**(1), 106–118 (2007)
9. De Prins, J.L., Schippers, F.K.M., Mulder, M., Paassen, R.V., In't Veld, A.C., Clarke, J.P.: Enhanced self-spacing algorithm for three-degree decelerating approaches. J. Guid. Control Dyn. **30**, 576–590 (2007)
10. Gouverneur, B., Mulder, J., Paassen, R.V., Stroosma, O.: Optimization of the SIMONA research simulator's motion filter settings for handling qualities experiments. In: AIAA Modeling and Simulation Technologies Conference (2003)
11. Field, E.J., Pinney, T.R., Paassen, R.V., Stroosma, O., Rivers, R.A.: Effects of implementation variations on the results of piloted simulator handling qualities evaluations. In: AIAA Modeling and Simulation Technologies Conference (2004)
12. Lam, T.M., Mulder, M., Paassen, R.V., Mulder, J.: Comparison of control and display augmentation for perspective flight-path displays. J. Guid. Control Dyn. **29**, 564–578 (2006)
13. Mulder, M., Veldhuijzen, A.R., Paassen, R.V., Mulder, J.: Integrating Fly-by-Wire controls with perspective flight-path displays. J. Guid. Control Dyn. **28**, 1263–1274 (2005)
14. Stroosma, O., Smaili, H., Lombaerts, T., Mulder, B.: Piloted simulator evaluation of new fault-tolerant flight control algorithms for reconstructed accident scenarios. In: AIAA Modeling and Simulation Technologies Conference (2008)
15. Stroosma, O., Lombaerts, T., Smaili, H., Mulder, M.: Real-time assessment and piloted evaluation of fault tolerant flight control designs in the SIMONA research flight simulator. In: Edwards, C., Lombaerts, T., Smaili, H. (eds.), Fault Tolerant Flight Control of LNCIS, vol. 399, pp. 451–475. Springer, Heidelberg (2010)
16. Alwi, H., Edwards, C., Stroosma, O., Mulder, J.: Piloted sliding mode FTC simulator evaluation for the ELAL Flight 1862 incident. In: AIAA Guidance, Navigation and Control Conference and Exhibit (2008)
17. Lombaerts, T., Smaili, H., Stroosma, O., Chu, Q.P., Mulder, J., Joosten, D.A.: Piloted simulator evaluation results of new fault-tolerant flight control algorithm. J. Guid. Control Dyn. **32**(6), 1747–1765 (2009)
18. Alwi, H., Edwards, C., Stroosma, O., Mulder, J.: Fault tolerant sliding mode control design with Piloted Simulator Evaluation. J. Guid. Control Dyn. **31**(5), 1186–1201 (2008)
19. Alwi, H., Edwards, C., Stroosma, O., Mulder, J.: Sliding-mode propulsion-control tests on a motion flight simulator. J. Guid. Control Dyn. **38**(4), 671–684 (2014)